



Basin-scale partitioning of Greenland ice sheet mass balance components (2007–2011)



M.L. Andersen^{a,*}, L. Stenseng^b, H. Skourup^b, W. Colgan^a, S.A. Khan^b, S.S. Kristensen^b, S.B. Andersen^a, J.E. Box^a, A.P. Ahlstrøm^a, X. Fettweis^c, R. Forsberg^b

^a Geological Survey of Denmark and Greenland (GEUS), Copenhagen DK-1350, Denmark

^b DTU Space, Lyngby DK-2800, Denmark

^c University of Liège, Department of Geography, 4000 Liège, Belgium

ARTICLE INFO

Article history:

Received 19 May 2014

Received in revised form 9 October 2014

Accepted 11 October 2014

Available online xxxx

Editor: P. Shearer

Keywords:

Greenland ice sheet
surface mass balance
ice discharge
airborne survey
flux gate
mass loss partition

ABSTRACT

The current deficit in Greenland ice sheet mass balance is due to both a decrease in surface mass balance (SMB) input and an increase in ice discharge (D) output. While SMB processes are beginning to be well captured by observationally-constrained climate modeling, insight into D is relatively limited. We use InSAR-derived velocities, in combination with ice thickness observations, to quantify the mass flux (F) across a flux perimeter around the ice sheet at ~ 1700 m elevation. To quantify D , we correct F for SMB, as well as changes in volume due to ice dynamics, in the area downstream of the gate. Using a 1961–1990 reference climatology SMB field from the MAR regional climate model, we quantify ice sheet mass balance within eighteen basins. We find a 2007–2011 mean D of 515 ± 57 Gt yr^{−1}. We find a 2007–2011 mean total mass balance of -262 ± 21 Gt yr^{−1}, which is equal to a 0.73 mm yr^{−1} global sea level rise contribution. This mass loss is dominated by SMB, which accounts for 61% of mass loss in the basins where partitioning is possible.

© 2014 Elsevier B.V. All rights reserved.

1. Introduction

The mass balance of the Greenland ice sheet is believed to have been in near-equilibrium until the early 1990s (Zwally et al., 2005; Rignot et al., 2008). Over the past two decades, however, the mass balance has become increasingly negative. Far more mass is now lost each year from surface melt water runoff and sublimation, as well as iceberg calving, than is gained from precipitation (Rignot et al., 2008; van den Broeke et al., 2009). In the past decade, Greenland's rate of ice loss has been the largest since 1840 (Box and Colgan, 2013). To understand the physical processes responsible for the mass deficit, ice sheet mass balance is generally viewed in terms of two components: the thermo-mechanical ice flow or iceberg discharge portion (D), and the climatic surface mass balance portion (SMB). While the distribution of contemporary mass loss was approximately equally split between both components during the 2000–2008 period (van den Broeke et al., 2009), since 2009 decreases in SMB have been responsible for $\sim 2/3$ of mass loss (Enderlin et al., 2014). Recent studies suggest total Greenland mass loss is currently ~ 260 Gt yr^{−1} (Rignot et al., 2008, year 2007;

Sasgen et al., 2012, period 2003–2009; Shepherd et al., 2012, period 2005–2010), which is equivalent to an ~ 0.72 mm yr^{−1} global sea level rise contribution. While SMB is intimately linked to climate, D has been shown to be sensitive to climate changes on a variety of spatial and temporal scales (Stearns and Hamilton, 2007; Andersen et al., 2010; Joughin et al., 2010b). The environmental forcing mechanism triggering increased D is not well understood at present, making projections of future D less well constrained than projections of future SMB (Pfeffer et al., 2008).

Here, we present basin-scale estimates of Greenland ice sheet mass balance in the years 2007 and 2011. To assess the SMB and D components of mass balance in each basin, we draw on (i) airborne ice thickness measurements carried out by the PROMICE program (www.promice.dk), (ii) InSAR-derived ice surface velocity fields generated by the NASA MEaSUREs program, and (iii) SMB fields generated by the regional climate model MAR. Similar to Rignot and Kanagaratnam (2006) and Rignot et al. (2008), we estimate the solid ice flux across a flux perimeter extending around the entire ice sheet. We correct this flux for downstream effects, between the flux gate and the grounding line, in order to derive the grounding line ice discharge. We then solve for mass balance by comparing this peripheral ice discharge to spatially integrated SMB. We compute both components of mass balance in eighteen major ice sheet drainage basins delineated by Zwally et al. (2012).

* Corresponding author.

E-mail address: mola@geus.dk (M.L. Andersen).

2. Data and methods

In the summers of 2007 and 2011 PROMICE conducted airborne radar and LiDAR surveys around the perimeter of the Greenland ice sheet in order to resolve high accuracy ice thickness. By design, the flight paths were nearly identical in both years (Fig. 1). We define 30 m wide flux gate sections along the repeat flight path. This uniform section width is defined by the spatial resolution of interpolated ice thickness data. These flux gates circumscribe the ice sheet at a mean elevation of ~ 1700 m, with the mean elevation of flux gate sections within individual basins ranging from ~ 1000 to ~ 2500 m. Similar to Thomas et al. (2000), flux gate sections are highest in East Greenland, where peripheral topography is complex. Where ice thickness cannot be resolved by our airborne survey, we interpolate ice thickness from the Ice2Sea digital elevation model (Bamber et al., 2013). These interpolated portions of the total flux perimeter comprise 26% and 36% for 2007 and 2011, respectively (see Supplementary Online Materials, Fig. S1, Table S1). Gate-perpendicular ice flux is quantified by multiplying this observed ice thickness with observed ice surface velocity.

MEaSURES InSAR- and TerraSAR-X-derived Greenland ice surface velocity fields are available for the winters of 2000–2001, 2005–2006, 2006–2007, 2007–2008, and 2008–2009 (Joughin et al., 2010a). Data for selected regions of Greenland are also available for years 2009–2011 (Joughin et al., 2011). Where possible, 2007 (2011) flux gate section velocities are interpolated from the 2006–2007 (2009–2011) velocity mosaic. In both 2007 and 2011, however, the velocity mosaics do not cover portions of the flux gate perimeter. At flux gate sections where velocity cannot be readily interpolated from an annual velocity mosaic, velocity is estimated via a temporal linear fit applied to all available years of velocity data at a given flux gate section. If, however, less than three years of velocity data are available, or the linear fit is assessed to be poor (i.e. correlation coefficient below 0.7), flux gate section velocity is interpolated from the velocity mosaic of the closest year with available data. Finally, at the small number of flux gate sections for which velocity data is not available in any year, a spatial linear interpolation is used to fill remaining gaps. At all gate sections, velocity is projected into gate-perpendicular vectors prior to multiplication with the thickness data. Velocity uncertainties ($\sigma_{v_{insar}}$) are quantified for the four methods as i) directly interpolated from the published error values, ii) the 95% confidence interval on the linear fit through the available years, iii) the published error value for the relevant year summed with the basin-mean of the linear fit SEE (Standard Error of the Estimate) added, and iv) 20% of the spatially interpolated velocities (see Supplementary Online Materials, Figs. S1, S2, and S3).

Three SMB fields are obtained from the Modèle Atmosphérique Régional (MAR) version 3.5 regional climate model, interpolated from 25×25 km to a 5×5 km grid (Fettweis et al., 2013): i) annual SMB-field for 2007, ii) annual SMB field for 2011, and iii) a mean field for the 1961–1990 reference climatology period. The MAR model is driven by ERA-40 re-analysis data up to 1978 and ERA-Interim afterwards. The uncertainty in SMB at basin scale is taken to be $\pm 20\%$ (see Supplementary Online Materials, Figs. S4 and S5). For comparison, we also employ annual SMB products reconstructed from meteorological station records, ice cores, and regional climate model output (Box, 2013).

We estimate the ice flux through a flux gate section (F_{sec}) with length (L) of 30 m and ice thickness H as:

$$F_{sec} = v f H L \rho \quad (1)$$

where v is gate-perpendicular ice surface velocity and f is the mean ratio of surface to depth-averaged velocity from Thomas et al. (2000), which is taken as 0.93 ± 0.05 . For flux gate sections

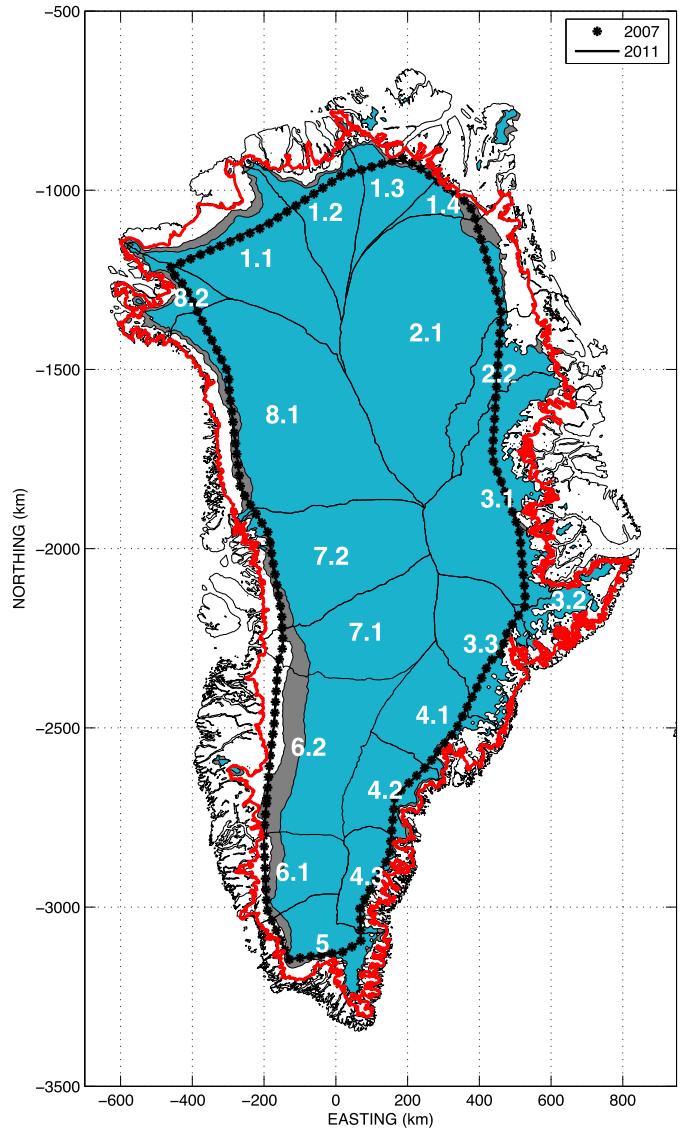


Fig. 1. Flight paths of the 2007 and 2011 airborne thickness surveys used to define the flux perimeter. White and blue areas within the ice sheet boundary (red line) denote ablation and accumulation areas, respectively, during the 1961–1990 period. Gray shading indicates areas that have transitioned from accumulation area (1961–1990) to ablation area by the 2007–2011 period.

upstream of the ELA (as determined by the reference climatology SMB field) bulk ice density ρ is assumed to be 830 kg m^{-3} in the top 25 m, reflecting firn (Harper et al., 2012), and 917 kg m^{-3} in the deeper ice column. For flux gate sections downstream of the ELA, ρ is set to 917 kg m^{-3} . Following Rignot and Kanagaratnam (2006), we calculate annual ice discharge (D) at the grounding line by correcting the ice flux through the flux gate using a reference period downstream SMB field (SMB_{ref}) that reflects the 1961–1990 average SMB. Unlike Rignot and Kanagaratnam (2006), we also apply a correction for the observed change in downstream ice storage due to glacier dynamics (ΔS). Both SMB_{ref} and ΔS are spatially integrated over the area downstream (ds) of the flux gate:

$$D = F + SMB_{ref,ds} - \Delta S_{ds} \quad (2)$$

where F is the flux integrated across all flux gate sections within a given basin. In this notation flux flowing downstream is positive.

The first two terms in Eq. (2) account for the flux input (F) to, and the mass change from surface mass balance ($SMB_{ref,ds}$) in, the ice sheet volume between the flux gate and the grounding line.

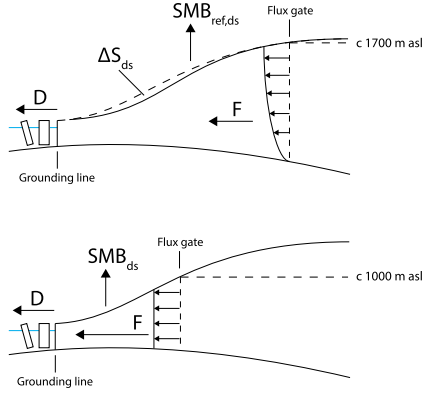


Fig. 2. Diagram showing differences in methodology between this study and others (e.g., Rignot and Kanagaratnam, 2006; Rignot et al., 2008). Top: The higher elevation of the flight line necessitates a downstream correction term reflecting the change in ice storage due to glacier dynamics (ΔS_{ds}). Bottom: The closer proximity of the fluxgates used in Rignot and Kanagaratnam (2006) to the grounding line allows the term describing the change in volume due to dynamics to be ignored. In both cases an SMB correction is applied to the F flux to adjust the upstream mass flux for surface processes. This study also applies a mean ratio of surface to depth-averaged velocity of 0.93, taken from Thomas et al. (2000), whereas Rignot and Kanagaratnam (2006), Rignot et al. (2008) assume plug flow.

The latter term (ΔS_{ds}) accounts for rate of change in ice storage between the flux gate and the grounding line. Other studies using similar methods have applied downstream SMB corrections corresponding to periods other than the 1961–1990 reference climatology, ranging from 1971–1988 (Rignot et al., 2008) to reference climatology fields with annual anomalies (van den Broeke et al., 2009; Sasgen et al., 2012). Here we follow Rignot and Kanagaratnam (2006). As the flux gates used in other studies (e.g., Rignot and Kanagaratnam, 2006; Rignot et al., 2008) are close to the grounding line, they assume that changes in downstream storage are small in comparison to the other two terms in Eq. (2). Furthermore, previous studies assume flow speed is constant throughout the ice column and equal to surface velocity (“plug flow”). As the PROMICE flux gate is located much farther inland from the grounding line, we acknowledge that downstream changes in ice geometry are non-trivial, and that plug flow cannot be assumed. Fig. 2 illustrates the differences in methodology between this and previous studies.

We estimate total mass balance downstream of the flux gate (ΔS_{ds}) from observations of rate of change in ice thickness using a combination of altimeter surveys (Khan et al., 2014). These include (i) NASA ATM flights from 2007 to 2011 (Krabbill, 2012), (ii) Ice, Cloud and land Elevation Satellite (ICESat) data from 2007 to 2009 (Zwally et al., 2011b), (iii) Land, Vegetation and Ice Sensor (LVIS) data from 2007 to 2011 (Blair and Hofton, 2012), and (iv) radar altimeter measurements from ENVISAT from 2007 to March 2011 (ESA, 2007). As radar altimetry suffers from problems with slope (ESA, 2007), we do not use radar data in the peripheral 50–70 km of the ice sheet. Moreover, we initially estimate elevation change rates from ENVISAT and laser altimetry separately, and then combine the independent rates.

Observed surface elevation changes are converted into ΔS_{ds} by applying a firn compaction correction, along with corrections for elastic uplift, glacial isostatic rebound (GIA) and SMB using the procedure described in Kjeldsen et al. (2013), yielding a 2007–2011 mean ΔS_{ds} field that isolates the component of downstream volume change due to glacier dynamics. Annual variability is assumed to be small on basin scale, as found by Khan et al. (2014), which allows the mean value from all available data to be employed for both 2007 and 2011.

Following Rignot et al. (2008) annual total ice sheet mass balance (TMB) is computed by subtracting annual D from the SMB field:

$$TMB = SMB - D \quad (3)$$

where SMB is the annual SMB field for 2007 or 2011.

The error in our F_{sec} calculations is estimated as the quadratic sum of the fractional uncertainties (σ) of the individual terms: H , f , v , and ρ , multiplied by the estimated flux F_{sec} (Eq. (4)). Uncertainties in ice thickness (H) stem from measurement errors in the LiDAR surface elevation ($\sigma h_{surf} = 0.1$ m) and radar bed elevation ($\sigma h_{bed} = 80$ m), which we sum in quadrature: $\sigma H = \sqrt{\sigma h_{surf}^2 + \sigma h_{bed}^2}$. Uncertainties in the InSAR velocities stem from two sources: Uncertainty associated with InSAR-derived ice surface velocities (formal and interpolation, combined in σv_{insar}) and a seasonal velocity cycle of less than 2% at high elevations ($\sigma v_{season} = 0.02v$, Doyle et al., 2014). Similar to uncertainties in ice thickness, these uncertainties in velocity are summed in quadrature: $\sigma v = \sqrt{\sigma v_{insar}^2 + \sigma v_{season}^2}$. We also assign a $\pm 5\%$ uncertainty in bulk ice density ($\sigma \rho$) from the prescribed weighted average. Finally, we assume the uncertainty of the mean ratio $f = 0.93$ of surface to depth-averaged velocity is 0.05 (Thomas et al., 2000). Thus, the error on the ice flux through a flux gate section (σF_{sec}) is:

$$\sigma F_{sec} = F_{sec} \sqrt{\left(\frac{\sigma H}{H}\right)^2 + \left(\frac{\sigma \rho}{\rho}\right)^2 + \left(\frac{\sigma f}{f}\right)^2 + \left(\frac{\sigma v}{v}\right)^2} \quad (4)$$

The errors on the individual sections, σF_{sec} , are summed within each basin. For ice sheet-wide estimates, we assume basins are independent and therefore add the uncertainties associated with D , F , and TMB in quadrature (Colgan et al., 2008).

While InSAR velocities are bedrock-controlled near the ice sheet margin, InSAR velocities become progressively less controlled towards the interior of the ice sheet, and ultimately constrained to c. 1995 in situ velocities collected along the 2000 m contour (Thomas et al., 2000). InSAR velocities along the PROMICE flight-line may therefore be biased towards the 1995 in situ velocities, and thus not reflect recent velocity changes in the ice sheet interior (Joughin et al., 2010b).

3. Results

Varying ice regimes are encountered around the flight line perimeter, with the dynamic regions (e.g. 7.1, Jakobshavn Isbræ, 4.1, Helheim Glacier) clearly characterized by larger fluxes. Summing all contributions from the eighteen basins in 2007 and 2011 yields total F values of 395 ± 68 and 399 ± 79 Gt yr⁻¹, respectively (Table 1). The corresponding MAR simulated SMB values for the reference period integrated within the flux gate perimeter is 438 ± 44 Gt yr⁻¹ indicating a positive, but non-significant, mass balance of the ice sheet interior of 43 ± 81 and 39 ± 91 Gt yr⁻¹ for 2007 and 2011, respectively. Employing the reconstructed SMB product based on in situ observations (Box, 2013) yields analogous interior mass balance values of 12 ± 76 and 7 ± 86 Gt yr⁻¹, respectively. Our interior mass balance observations carry large error estimates due to compounding the errors associated with both mass budget components.

The calculated D fluxes using MAR are listed in Table 1 at basin scale. Total ice sheet D for the years 2007 and 2011 is 512 ± 76 and 517 ± 85 Gt yr⁻¹, respectively. Between 2007 and 2011 Jakobshavn drainage (7.1) on the West Coast accelerated slightly, as did Helheim Glacier drainage system (4.1) in the South East. Basin 3.3 (Kangerlussuaq Glacier) was unchanged between the observation years.

Table 1

Quantities used for estimates of grounding line solid ice discharge (D), all in Gt yr^{-1} : mass flux at flux gate perimeter (F), 1961–1990 reference period MAR derived SMB for the area between flux gate and grounding line (SMB_{ds}), and 2007–2011 mean downstream change in storage due to glacier dynamics (ΔS_{ds}).

Basin	F 2007	F 2011	SMB_{ds} Ref.	ΔS_{ds} 2007–2011	D 2007	D 2011
1.1	14 ± 1	15 ± 3	−3 ± 0.5	2 ± 0.5	9 ± 2	9 ± 3
1.2	5 ± 1	5 ± 2	−1 ± 0.1	2 ± 0.3	3 ± 1	3 ± 2
1.3	3 ± 0	3 ± 1	0 ± 0.0	−1 ± 0.5	4 ± 1	4 ± 1
1.4	1 ± 0	1 ± 1	−1 ± 0.1	−1 ± 0.1	2 ± 0	2 ± 1
2.1	26 ± 3	27 ± 3	−5 ± 0.7	−6 ± 0.5	27 ± 3	28 ± 4
2.2	2 ± 0	2 ± 1	2 ± 0.3	−2 ± 0.4	6 ± 1	6 ± 1
3.1	16 ± 4	17 ± 6	12 ± 1.7	−6 ± 1.5	34 ± 5	34 ± 7
3.3	23 ± 4	23 ± 4	21 ± 3.0	−12 ± 0.6	56 ± 6	56 ± 6
4.1	27 ± 3	28 ± 3	4 ± 0.5	−11 ± 0.2	41 ± 3	43 ± 3
4.2	39 ± 10	39 ± 8	12 ± 1.7	−2 ± 0.1	53 ± 10	53 ± 9
4.3	28 ± 8	28 ± 7	7 ± 1.0	−7 ± 0.2	42 ± 9	41 ± 7
5.0	17 ± 8	17 ± 9	3 ± 0.4	−7 ± 0.8	27 ± 8	27 ± 9
6.1	12 ± 4	13 ± 6	−8 ± 1.1	−5 ± 0.3	9 ± 4	10 ± 6
6.2	30 ± 4	29 ± 6	−19 ± 2.7	−7 ± 0.3	17 ± 6	17 ± 7
7.1	36 ± 4	38 ± 4	−3 ± 0.5	−7 ± 0.0	40 ± 4	42 ± 4
7.2	46 ± 5	46 ± 6	−4 ± 0.6	−8 ± 0.1	50 ± 5	50 ± 6
8.1	67 ± 7	67 ± 9	−1 ± 0.2	−19 ± 0.3	85 ± 7	84 ± 9
8.2	2 ± 0	2 ± 1	2 ± 0.3	−3 ± 0.3	8 ± 1	7 ± 1
Total	395 ± 68	399 ± 79	16 ± 15	−101 ± 7	512 ± 76	517 ± 85

Table 2

Quantities used for estimating total mass balance (TMB), all in Gt yr^{-1} : MAR derived annual SMB fields and solid ice discharge values (D ; from Table 1).

Basin	SMB_{year} 2007	SMB_{year} 2011	D 2007	D 2011	TMB 2007	TMB 2011
1.1	−1 ± 0	−5 ± 1	9 ± 2	9 ± 3	−10 ± 2	−14 ± 3
1.2	5 ± 1	0 ± 0	3 ± 1	3 ± 2	2 ± 1	−2 ± 2
1.3	4 ± 1	0 ± 0	4 ± 1	4 ± 1	0 ± 1	−4 ± 1
1.4	−1 ± 0	−2 ± 0	2 ± 0	2 ± 1	−2 ± 0	−3 ± 1
2.1	16 ± 3	17 ± 3	27 ± 3	28 ± 4	−11 ± 4	−11 ± 5
2.2	4 ± 1	4 ± 1	6 ± 1	6 ± 1	−2 ± 1	−1 ± 1
3.1	21 ± 4	39 ± 8	34 ± 5	34 ± 7	−12 ± 7	5 ± 10
3.3	40 ± 8	52 ± 10	56 ± 6	56 ± 6	−16 ± 10	−5 ± 12
4.1	30 ± 6	32 ± 6	41 ± 3	43 ± 3	−11 ± 7	−11 ± 7
4.2	39 ± 8	40 ± 8	53 ± 10	53 ± 9	−14 ± 13	−13 ± 12
4.3	28 ± 6	27 ± 5	42 ± 9	41 ± 7	−14 ± 10	−14 ± 9
5.0	7 ± 1	5 ± 1	27 ± 8	27 ± 9	−19 ± 8	−22 ± 9
6.1	−3 ± 1	−3 ± 1	9 ± 4	10 ± 6	−12 ± 4	−13 ± 6
6.2	−22 ± 4	−27 ± 5	17 ± 6	17 ± 7	−39 ± 7	−44 ± 9
7.1	23 ± 5	15 ± 3	40 ± 4	42 ± 4	−18 ± 6	−27 ± 5
7.2	28 ± 6	18 ± 4	50 ± 5	50 ± 6	−22 ± 8	−32 ± 7
8.1	46 ± 9	39 ± 8	85 ± 7	84 ± 9	−39 ± 12	−46 ± 12
8.2	−6 ± 1	−7 ± 1	8 ± 1	7 ± 1	−14 ± 1	−14 ± 2
Total	259 ± 52	245 ± 49	512 ± 76	517 ± 85	−253 ± 29	−272 ± 31

We infer a 2007–2011 mean total mass balance (TMB) of $−262 ± 21 \text{ Gt yr}^{-1}$ (Table 2), corresponding to a global sea level rise contribution of $\sim 0.73 \text{ mm yr}^{-1}$.

4. Discussion

The mean ice sheet wide grounding line discharge (D) is $515 ± 57 \text{ Gt yr}^{-1}$. This is consistent with the values of 507 and 502 Gt yr^{-1} for 2006 and 2007 reported in Rignot et al. (2008), and also Enderlin et al. (2014), in which the total discharge from 178 outlet glaciers is estimated as 513 Gt yr^{-1} in 2007 and 544 Gt yr^{-1} in 2011.

Our 2007–2011 mean TMB of $−262 ± 21 \text{ Gt yr}^{-1}$ is more negative than Colgan et al. (2014) ($−217 ± 20 \text{ Gt yr}^{-1}$, 2003–2010), but $\sim 116 \text{ Gt yr}^{-1}$ less negative than the $−378 ± 50 \text{ Gt yr}^{-1}$ found by Enderlin et al. (2014) in 2009–2012. We note that Enderlin et al. (2014) include the peripheral glaciers and ice caps of the Geikie plateau, which we do not, and also include the extreme mass loss year of 2012 (Tedesco et al., 2013). The inclusion or exclusion of peripheral glaciers can account for up to 15% of Greenland's mass loss signal (Colgan et al., 2014). Our TMB agrees well with the

reconciled 2005–2010 Greenland TMB value of $−264 ± 30 \text{ Gt yr}^{-1}$ reported in Shepherd et al. (2012) and with the $−191 ± 23 \text{ Gt yr}^{-1}$ to $−240 ± 28 \text{ Gt yr}^{-1}$ mass loss found by Sørensen et al. (2011) for the period 2003–2008. Due to an acceleration in TMB over the last two decades (Rignot et al., 2011), differences in observation period likely play an important role in explaining the apparent discrepancies between studies. Furthermore, differences in the data sets used for quantifying ice thickness, velocity, the magnitude and distribution of interpolation, and the SMB products used for downstream F corrections, all influence the final mass balance estimates, and are different for the studies discussed.

Considering the high-elevation regions ($>2000 \text{ m a.s.l.}$), the consensus appears to be an ongoing mass gain: Zwally et al. (2011a) infers a decrease in the rate of mass gain in the interior from 44 Gt yr^{-1} to 28 Gt yr^{-1} between the periods 1992–2002 and 2003–2007. Luthcke et al. (2006) find a high-elevation mass gain of $\sim 54 \text{ Gt yr}^{-1}$ in the years 2003–2005. Our 2007–2011 mean positive interior mass balance (IMB) of $41 ± 61 \text{ Gt yr}^{-1}$ is consistent with both of these, but carries large error estimates. Thomas et al. (2000) and Krabill et al. (2000) found the $>2000 \text{ m}$ regions to be in balance on average in the years 1993–1997 and

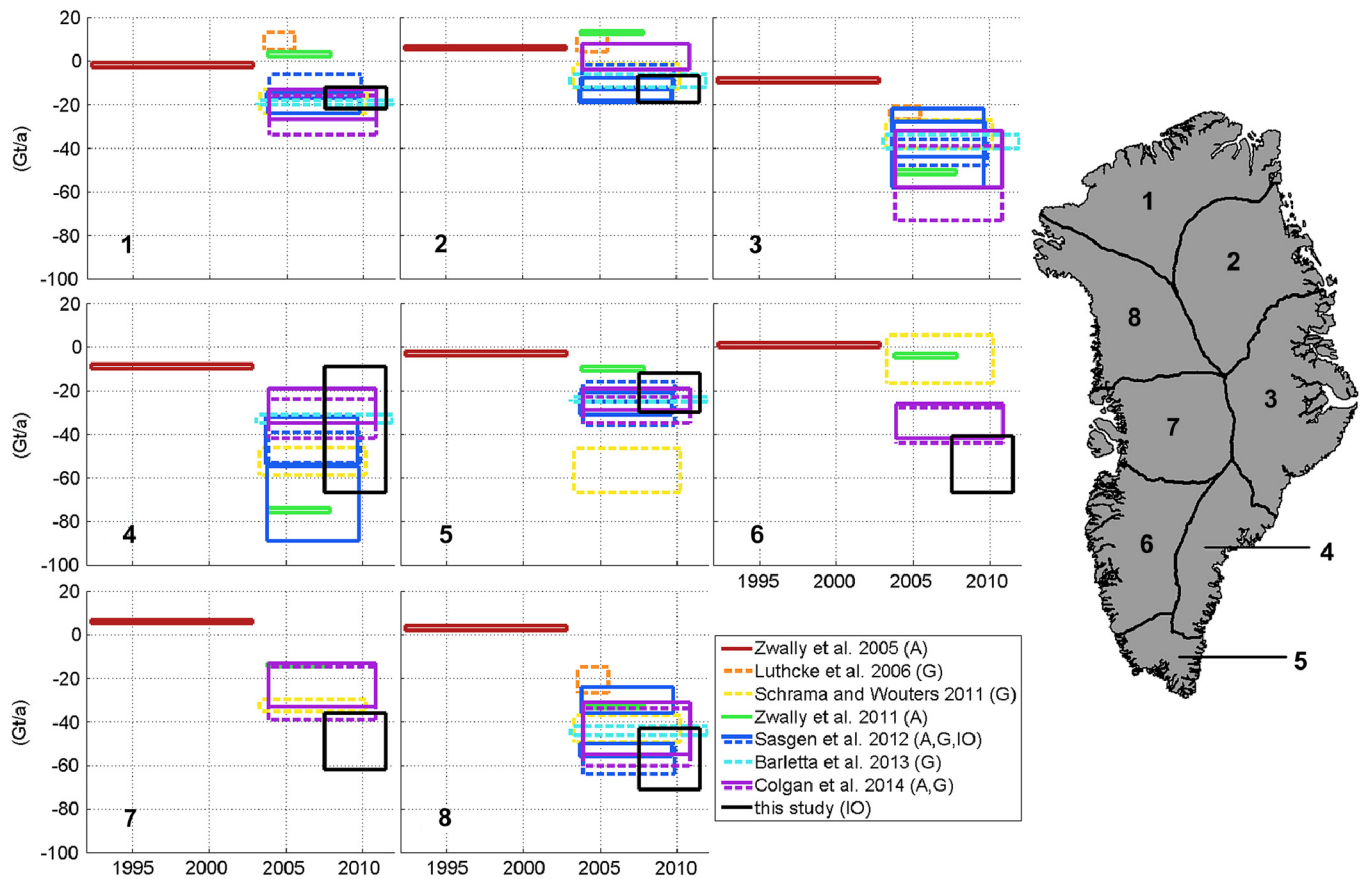


Fig. 3. Mass balance estimates for Greenland's eight major drainage basins (inset) derived through altimetry (A), gravimetry (G) and input–output (IO) approaches (Zwally et al., 2005, 2011a; Luthcke et al., 2006; Schrama and Wouters, 2011; Sasgen et al., 2012; Barletta et al., 2013; Colgan et al., 2014). The horizontal extent of each box denotes observation period, while the vertical extent denotes reported uncertainty. Solid lines denote estimates for the ice sheet proper, while dashed lines denote estimates that include peripheral glaciers.

1994–1999. Later studies suggest slight high-elevation thinning between 1997 and 2002–2003 (Krabill et al., 2004), but are inconclusive. At ~ 1700 m a.s.l., our flight line is lower than the 2000 m contour typically employed in studies of high-elevation mass balance. Therefore, we include parts of the ablation zone in our IMB estimates (Fig. 1), introducing a negative bias relative to previous studies. We note that our computed F fluxes have not changed beyond uncertainty over our observation period, indicating that dynamic effects changing the geometry of the ice sheet between 2007 and 2011 are not detectable at the flight line elevation.

We compare our basin-scale mass loss assessment to previous basin-scale studies of: (i) the ice sheet proper (Zwally et al., 2005, 2011a), (ii) the ice sheet proper plus peripheral glaciers (Luthcke et al., 2006; Schrama and Wouters, 2011; Barletta et al., 2013) or (iii) a combination of both (Colgan et al., 2014; Fig. 3). Even considering the variation in SMB models used across other works (Vernon et al., 2013), the mass balance we assess is within the range of previous estimates in basins 1, 2, 4, 5, and 8, while it is lower than previous estimates in basins 6 and 7, although still within uncertainty of Colgan et al. (2014) in basin 6. Our exclusion of basin 3.2 prevents assessing a directly comparable basin 3 value. While we consistently assess similar or more mass loss than altimetry collected over the slightly earlier 2003 to 2009 period in all basins except 4, in South East Greenland, we underestimate mass loss relative to some gravimetry-based studies (Schrama and Wouters, 2011; Sasgen et al., 2012) in the southeast (basins 4 + 5) and overestimate mass loss relative to gravimetry in the southwest (basins 6 and 7). We speculate that this apparent shift in mass loss detected by gravimetry from South West to South East Green-

land, relative to our input–output assessment, may be due to aliasing of the gravimetry signal within the relatively narrow basins 4 and 5. Altimetry, gravimetry and input–output methods appear to agree best in Northwest Greenland (basin 8), where they document progressively negative mass balance since 1992. Perhaps the overarching message of this basin-scale inter-comparison is that aside from basins 2 and 3, the consensus is that all major drainage basins exhibit substantially negative mass balance with formal uncertainties being substantially smaller than inter-comparison discrepancies, even considering the differences in methodology and data sets employed.

The basin-scale mass loss we assess may be partitioned into SMB and D components in twelve of the eighteen ice sheet basins where the majority of mass loss occurs ($\sim 73\%$ of total ice sheet mass loss). The partition of mass loss cannot be resolved beyond uncertainty in four of the remaining basins, and mass balance is within uncertainty zero in two basins (Fig. 4). We attribute the majority of the ice sheet's current mass loss to West Greenland (basins 6.1 through 8.2 $\sim 61\%$ of total ice sheet mass loss). We note that basin 8.1, comprising several marine terminating glacier complexes (e.g., Upernavik Ice Stream) is presently the single largest source of ice sheet-derived sea level rise ($\sim 16\%$ of total ice sheet mass loss), closely followed by basin 6.2, in which the ice sheet is primarily land terminating, with a large SMB related mass loss. We observe high dynamic fractions of mass loss in basins 2.1, 3.3, 7.1, 7.2, and 8.1. Qualitatively this is consistent with the strong outlet glacier acceleration observed in some of these areas in the past two decades (Luckman et al., 2006; Stearns and Hamilton, 2007; Pritchard et al., 2009). Across the basins for which mass loss can

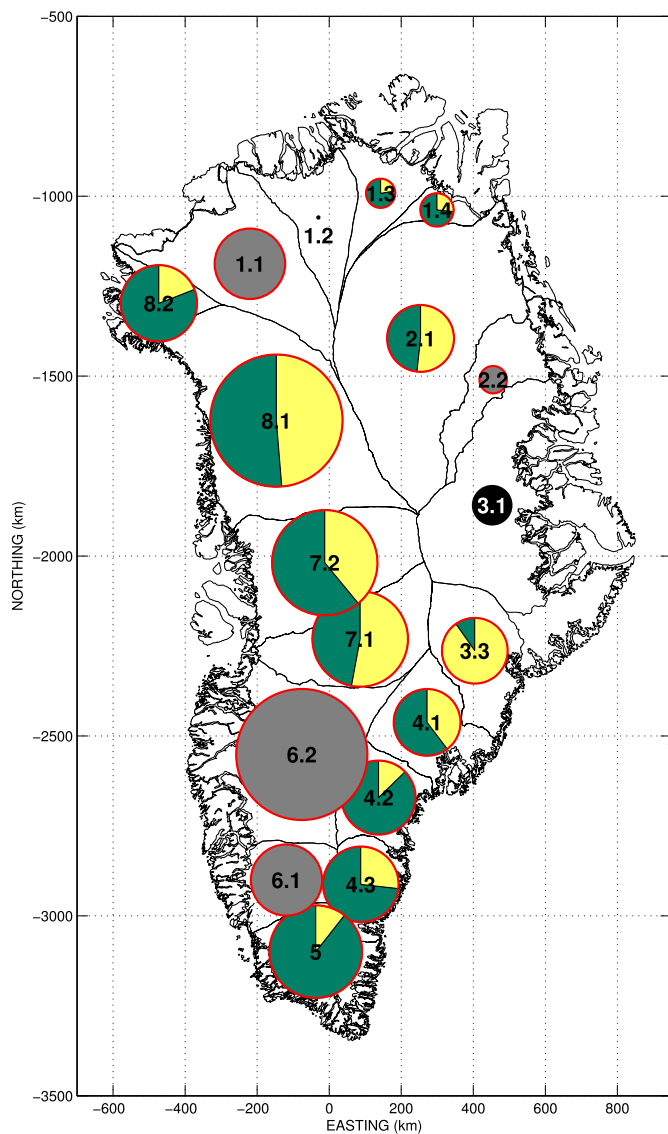


Fig. 4. Partition of 2007–2011 mean mass loss into surface mass balance (dark green) and ice dynamics (yellow) components. Gray circles denote basins in which the partition of mass balance components is not possible. Circle size is proportional to total mass balance. Red perimeters indicate negative total mass balance. Black circles indicate mass balance of zero within uncertainty. Numbers indicate basin names.

be partitioned with confidence, mass loss due to SMB comprises 61% of total mass loss. This falls between the ~50% SMB contribution reported by van den Broeke et al. (2009) over the 2000–2008 period, and the 68% SMB contribution reported by Enderlin et al. (2014) over the 2009–2012 period.

5. Conclusion

We estimate ice fluxes across a flux gate perimeter following the ~1700 m a.s.l. contour of the Greenland ice sheet for the years 2007 and 2011. We integrate a 1961–1990 reference period SMB field within the flux gate perimeter and estimate the interior mass balance to be $41 \pm 61 \text{ Gt yr}^{-1}$, i.e. zero within uncertainty. This result is concordant with previous studies (e.g. Thomas et al., 2000; Krabill et al., 2000) that find that the interior of the Greenland ice sheet to be in neutral or slightly positive mass balance. Using reference period SMB values, and corrections for the dynamic volume change downstream of the flux gate, we infer the ice discharge at the grounding line, D . The total D value (mean 2007–2011 value

of $515 \pm 57 \text{ Gt yr}^{-1}$) is consistent with values found in other studies. We then derive the mean 2007–2011 total mass balance for the whole ice sheet on basin level. Here we find that the ice sheet total ($-262 \pm 21 \text{ Gt yr}^{-1}$) agrees well with other studies, but the reconciliation of the spatial distribution to other works is less obvious.

Acknowledgements

PROMICE is funded by the Danish Ministry of Climate, Energy and Building, and is operated by the Geological Survey of Denmark and Greenland (GEUS). This publication is contribution number 45 of the Nordic Centre of Excellence SVALI, “Stability and Variations of Arctic Land Ice”, funded by the Nordic Top-level Research Initiative (TRI). WC was supported by DFF FNU grant No. 11-115166. We acknowledge Dr. Ian Joughin, University of Washington, for making published and unpublished velocity data available for the study. We would also like to thank two anonymous reviewers and editor Dr. Peter Shearer, for their thorough reviews and very valuable comments, which have significantly improved the manuscript.

Appendix A. Supplementary material

Supplementary material related to this article can be found online at <http://dx.doi.org/10.1016/j.epsl.2014.10.015>.

References

- Andersen, M.L., Larsen, T.B., Nettles, M., Elsoegui, P., van As, D., Hamilton, G.S., Stearns, L.A., Davis, J.L., Ahlström, A.P., de Juan, J., Ekström, G., Stenseng, L., Khan, S.A., Forsberg, R., Dahl-Jensen, D., 2010. Spatial and temporal melt variability at Helheim Glacier, East Greenland, and its effect on ice dynamics. *J. Geophys. Res., Earth Surf.* 115.
- Bamber, J.L., Griggs, J.A., Hurkmans, R.T.W.L., Dowdeswell, J.A., Gogineni, S.P., Howat, I., Mouginot, J., Paden, J., Palmer, S., Rignot, E., Steinhage, D., 2013. A new bed elevation dataset for Greenland. *The Cryosphere* 7 (2), 499–510.
- Barletta, V.R., Sørensen, L.S., Forsberg, R., 2013. Scatter of mass changes estimates at basin scale for Greenland and Antarctica. *The Cryosphere* 7 (5), 1411–1432.
- Blair, B., Hofton, M., 2012. IceBridge LVIS L2 Geolocated ground elevation and return energy quartiles. Digital media. <http://nsidc.org/data/ilvis2.html>.
- Box, J.E., 2013. Greenland ice sheet mass balance reconstruction. Part II: surface mass balance (1840–2010). *J. Climate* 26 (18), 6974–6989.
- Box, J.E., Colgan, W., 2013. Greenland ice sheet mass balance reconstruction. Part III: marine ice loss and total mass balance (1840–2010). *J. Climate* 26 (18), 6990–7002.
- Colgan, W., Davis, J., Sharp, M., 2008. Is the high-elevation region of Devon Ice Cap thickening? *J. Glaciol.* 54 (186), 428–436.
- Colgan, W., Abdalati, W., Citterio, M., Csatho, B., Fettweis, X., Luthcke, S., Moholdt, G., Stober, M., 2014. Hybrid inventory, gravimetry and altimetry (HIGA) mass balance product for Greenland and the Canadian Arctic. *Cryosph. Discuss.* 8, 537–580.
- Doyle, S.H., Hubbard, A., Fitzpatrick, A.A.W., van As, D., Mikkelsen, A.B., Pettersson, R., Hubbard, B., 2014. Persistent flow acceleration within the interior of the Greenland ice sheet. *Geophys. Res. Lett.* 41.
- Enderlin, E.M., Howat, I.M., Jeong, S., Noh, M.-J., van Angelen, J.H., van den Broeke, M.R., 2014. An improved mass budget for the Greenland ice sheet. *Geophys. Res. Lett.* 41 (3), 866–872.
- ESA, 2007. ENVISAT RA2/MWR Product Handbook. European Space Agency.
- Fettweis, X., Franco, B., Tedesco, M., van Angelen, J.H., Lenaerts, J.T.M., van den Broeke, M.R., Gallee, H., 2013. Estimating the Greenland ice sheet surface mass balance contribution to future sea level rise using the regional atmospheric climate model MAR. *The Cryosphere* 7 (2), 469–489.
- Harper, J., Humphrey, N., Pfeffer, W.T., Brown, J., Fettweis, X., 2012. Greenland ice-sheet contribution to sea-level rise buffered by meltwater storage in firn. *Nature* 491 (7423), 240–243.
- Joughin, I., Smith, B., Howat, I., Scambos, T., 2010a. MEASURES Greenland Ice Sheet Velocity Map from InSAR Data. <http://dx.doi.org/10.5067/MEASURES/CRYOSPHERE/nsidc-0481.001>.
- Joughin, I., Smith, B.E., Howat, I.M., Scambos, T., Moon, T., 2010b. Greenland flow variability from ice-sheet-wide velocity mapping. *J. Glaciol.* 56 (197), 415–430.
- Joughin, I., Smith, B., Howat, I., Scambos, T., 2011. MEASURES Greenland ice velocity: selected glacier site velocity maps from InSAR. <http://dx.doi.org/10.5067/MEASURES/CRYOSPHERE/nsidc-0481.001>.

- Khan, S.A., Kjær, K.H., Bevis, M., Bamber, J.L., Wahr, J., Kjeldsen, K.K., Bjørk, A.A., Korsgaard, N.J., Stearns, L.A., van den Broeke, M.R., Liu, L., Larsen, N.K., Muresan, I.S., 2014. Sustained mass loss of the northeast Greenland ice sheet triggered by regional warming. *Nat. Clim. Change* 4 (4), 292–299.
- Kjeldsen, K.K., Khan, S.A., Wahr, J., Korsgaard, N.J., Kjær, K.H., Bjørk, A.A., Hurkmans, R., van den Broeke, M.R., Bamber, J.L., van Angelen, J.H., 2013. Improved ice loss estimate of the northwestern Greenland ice sheet. *J. Geophys. Res., Solid Earth* 118 (2), 698–708.
- Krabill, W.B., 2012. IceBridge ATM L2 icesn elevation, slope, and roughness, [1993–2012]. Digital media. <http://nsidc.org/data/ilatm2.html>.
- Krabill, W., Abdalati, W., Frederick, E., Manizade, S., Martin, C., Sonntag, J., Swift, R., Thomas, R., Wright, W., Yungel, J., 2000. Greenland ice sheet: high-elevation balance and peripheral thinning. *Science* 289 (5478), 428–430.
- Krabill, W., Hanna, E., Huybrechts, P., Abdalati, W., Cappelen, J., Csatho, B., Frederick, E., Manizade, S., Martin, C., Sonntag, J., Swift, R., Thomas, R., Yungel, J., 2004. Greenland ice sheet: increased coastal thinning. *Geophys. Res. Lett.* 31 (24).
- Luckman, A., Murray, T., de Lange, R., Hanna, E., 2006. Rapid and synchronous ice-dynamic changes in East Greenland. *Geophys. Res. Lett.* 33 (3).
- Luthcke, S.B., Zwally, H.J., Abdalati, W., Rowlands, D.D., Ray, R.D., Nerem, R.S., Lemoine, F.G., McCarthy, J.J., Chinn, D.S., 2006. Recent Greenland ice mass loss by drainage system from satellite gravity observations. *Science* 314 (5803), 1286–1289.
- Pfeffer, W.T., Harper, J.T., O'Neel, S., 2008. Kinematic constraints on glacier contributions to 21st-century sea-level rise. *Science* 321 (5894), 1340–1343.
- Pritchard, H.D., Arthern, R.J., Vaughan, D.G., Edwards, L.A., 2009. Extensive dynamic thinning on the margins of the Greenland and Antarctic ice sheets. *Nature* 461 (7266), 971–975.
- Rignot, E., Kanagaratnam, P., 2006. Changes in the velocity structure of the Greenland ice sheet. *Science* 311 (5763), 986–990.
- Rignot, E., Box, J.E., Burgess, E., Hanna, E., 2008. Mass balance of the Greenland ice sheet from 1958 to 2007. *Geophys. Res. Lett.* 35 (20).
- Rignot, E., Velicogna, I., van den Broeke, M.R., Monaghan, A., Lenaerts, J., 2011. Acceleration of the contribution of the Greenland and Antarctic ice sheets to sea level rise. *Geophys. Res. Lett.* 38.
- Sasgen, I., van den Broeke, M., Bamber, J.L., Rignot, E., Sørensen, L.S., Wouters, B., Martinec, Z., Velicogna, I., Simonsen, S.B., 2012. Timing and origin of recent regional ice-mass loss in Greenland. *Earth Planet. Sci. Lett.* 333, 293–303.
- Schrama, E.J.O., Wouters, B., 2011. Revisiting Greenland ice sheet mass loss observed by GRACE. *J. Geophys. Res., Solid Earth* 116.
- Shepherd, A., Ivins, E.R., Geruo, A., Barletta, V.R., Bentley, M.J., Bettadpur, S., Briggs, K.H., Bromwich, D.H., Forsberg, R., Galin, N., Horwath, M., Jacobs, S., Joughin, I., King, M.A., Lenaerts, J.T.M., Li, J., Ligtenberg, S.R.M., Luckman, A., Luthcke, S.B., McMillan, M., Meister, R., Milne, G., Mouginot, J., Muir, A., Nicolas, J.P., Paden, J., Payne, A.J., Pritchard, H., Rignot, E., Rott, H., Sørensen, L.S., Scambos, T.A., Scheuchl, B., Schrama, E.J.O., Smith, B., Sundal, A.V., van Angelen, J.H., van de Berg, W.J., van den Broeke, M.R., Vaughan, D.G., Velicogna, I., Wahr, J., Whitehouse, P.L., Wingham, D.J., Yi, D., Young, D., Zwally, H.J., 2012. A reconciled estimate of ice-sheet mass balance. *Science* 338 (6111), 1183–1189.
- Sørensen, L.S., Simonsen, S.B., Nielsen, K., Lucas-Picher, P., Spada, G., Adalgeirsdottir, G., Forsberg, R., Hvidberg, C.S., 2011. Mass balance of the Greenland ice sheet (2003–2008) from ICESat data – the impact of interpolation, sampling and firn density. *The Cryosphere* 5 (1), 173–186.
- Stearns, L.A., Hamilton, G.S., 2007. Rapid volume loss from two East Greenland outlet glaciers quantified using repeat stereo satellite imagery. *Geophys. Res. Lett.* 34 (5).
- Tedesco, M., Fettweis, X., Mote, T., Wahr, J., Alexander, P., Box, J.E., Wouters, B., 2013. Evidence and analysis of 2012 Greenland records from spaceborne observations, a regional climate model and reanalysis data. *The Cryosphere* 7 (2), 615–630.
- Thomas, R., Akins, T., Csatho, B., Fahnestock, M., Gogineni, P., Kim, C., Sonntag, J., 2000. Mass balance of the Greenland ice sheet at high elevations. *Science* 289 (5478), 426–428.
- van den Broeke, M., Bamber, J., Ettema, J., Rignot, E., Schrama, E., van den Berg, W.J., 2009. Partitioning recent Greenland mass loss. *Science* 326, 984–986.
- Vernon, C.L., Bamber, J.L., Box, J.E., van den Broeke, M.R., Fettweis, X., Hanna, E., Huybrechts, P., 2013. Surface mass balance model intercomparison for the Greenland ice sheet. *The Cryosphere* 7 (2), 599–614.
- Zwally, H.J., Giovinetto, M.B., Li, J., Cornejo, H.G., Beckley, M.A., Brenner, A.C., Saba, J.L., Yi, D., 2005. Mass changes of the Greenland and Antarctic ice sheets and shelves and contributions to sea-level rise: 1992–2002. *J. Glaciol.* 51 (175), 509–527.
- Zwally, H.J., Li, J., Brenner, A.C., Beckley, M., Cornejo, H.G., Dimarzio, J., Giovinetto, M.B., Neumann, T.A., Robbins, J., Saba, J.L., Yi, D., Wang, W., 2011a. Greenland ice sheet mass balance: distribution of increased mass loss with climate warming; 2003–07 versus 1992–2002. *J. Glaciol.* 57 (201), 88–102.
- Zwally, H., Schutz, R., Bentley, C., Bufton, J., Herring, T., Minster, J., Spinhirne, J., Thomas, R., 2011b. GLAS/ICESat L2 Antarctic and Greenland ice sheet altimetry data V031. Digital media.
- Zwally, H., Giovinetto, M., Beckley, M., Saba, J., 2012. Antarctic and Greenland drainage systems, GSFC cryospheric sciences laboratory. http://icesat4.gsfc.nasa.gov/cryo_data/ant_grn_drainage_systems.php.